JOURNAL OF Materials CHEMISTRY

Synthesis, crystal chemistry, and electrical, oxygen permeation, and magnetic properties of $LaSr_3GaFe_{2-x}Co_xO_{10-\delta}$ ($0 \leqslant x \leqslant 2$ and $0 \leqslant \delta \leqslant 2$)

F. Prado,† K. Gurunathan and A. Manthiram*

Materials Science and Engineering Program, ETC 9.104, The University of Texas at Austin, Austin, TX 78712, USA. E-mail: rmanth@mail.utexas.edu

Received 18th April 2002, Accepted 30th May 2002
First published as an Advance Article on the web 2nd July 2002

The crystal chemistry and electrical, oxygen permeation, and magnetic properties of the $n = 3$ member of the Ruddlesden–Popper (R–P) series of phases $LaSr_3GaFe_{2-x}Co_xO_{10-\delta}$, with $0 \leqslant x \leqslant 2$ and $0 \leqslant \delta \leqslant 2$, have been investigated. While the orthorhombic cell parameters a and b and the unit cell volume decrease, the c parameter increases with increasing Co content. Conductivity measurements show that the samples exhibit a thermally activated process, with $0.17 \leqslant E_a \leqslant 0.35$ eV. The oxygen permeation flux values ($jO_2 \approx 1 \times 10^{-9}$ mol s^{-1} cm^{-2}) at 900 °C across 1.5 mm thick $LaSr_3GaFe_{2-x}Co_xO_{10-\delta}$ membranes are two orders of magnitude lower than those observed previously with other $n = 2$ and 3 R–P phases (tetragonal) due to the orthorhombic distortion and negligible oxygen vacancy concentration gradient across the membrane. The reduction of the $LaSr_3GaFe_{2-x}Co_xO_{10-\delta}$ phases in a mixture of 90% Ar and 10% H_2 leads to the formation of $LaSr_3GaFe_{2-x}Co_xO_{9-x/2}$ phases containing Co^{2+} and with orthorhombic symmetry. SQUID magnetometer data indicates antiferromagnetic interactions and the presence of high spin Co^{3+} ions in the $LaSr_3GaFe_{2-x}Co_xO_{9-x/2}$ phases.

Introduction

Mixed conductors exhibiting both oxide-ion and electronic conduction find applications as oxygen separation membranes[1] and as electrodes in solid oxide fuel cells.[2] Perovskite oxides such as $La_{1-x}Sr_xCo_{1-y}Fe_yO_{3-\delta}$ are the most widely investigated mixed conductors, as they exhibit both high oxide-ion and electronic conductivity.[3–5] However, intergrowth oxides based on perovskite-related structures, such as the Ruddlesden–Popper (R–P) series of phases $A_{n+1}B_nO_{3n+1}$ (A = rare earth or alkaline earth, B = transition metal, and $n = 1$, 2 and 3), have been investigated to a lesser extent. The crystal structures of the $A_{n+1}B_nO_{3n+1}$ phases are closely related to that of the perovskite phase, in which n is the number of ABO_3 perovskite blocks having corner-shared BO_6 octahedra alternating with AO rock-salt layers along the c-axis.[6] The ABO_3 perovskite phase belongs to the $n = \infty$ member of this series.

Strontium iron oxides with iron in the 3+/4+ oxidation states are known to form the $Sr_{n+1}Fe_nO_{3n+1}$ series of R–P phases. In this series, the $n = 1$ and 2 members have a tetragonal structure with nearly regular octahedral coordination for iron.[7,8] The $n = 3$ member, $Sr_4Fe_3O_{10}$, has also been reported by Brisi and Rolando[9] to have a tetragonal structure with the space group $I4/mmm$ (Fig. 1). However, the synthesis of $Sr_4Fe_3O_{10}$ results in the formation of the secondary phases $Sr_3Fe_2O_7$ and $SrFeO_3$.[9,10] Lee *et al.*[10] reported the stabilization of the pure $n = 3$ phase by a partial substitution of La^{3+} for Sr^{2+} with $0.96 < x < 1.04$ in $Sr_{4-x}La_xFe_3O_{10-\delta}$. They also reported a large degree of oxygen nonstoichiometry at high temperatures in air for $LaSr_3Fe_3O_{10-\delta}$ with $0 \leqslant \delta \leqslant 0.8$. More recently, Armstrong *et al.*[11] have reported the synthesis and oxygen permeation properties of $LaSr_3Fe_{3-x}Co_xO_{10-\delta}$ with $0 \leqslant x \leqslant 1.5$. While the substitution of Co for Fe was found to improve the electronic conductivity due to the increase in the covalency of the B(3d)–O(2p) bond, no significant changes were observed in the degree of oxygen nonstoichiometry. Nevertheless, the oxide-ion conductivity values obtained from oxygen permeation measurements were found to increase with increasing Co content.[11]

On the other hand, the substitution of Ga^{3+} for $Fe^{3+/4+}$ in $LaSr_3Fe_{3-x}Ga_xO_{10-\delta}$ was found to increase the oxygen nonstoichiometry and cause a structural transformation from tetragonal to orthorhombic symmetry.[12] The solubility range

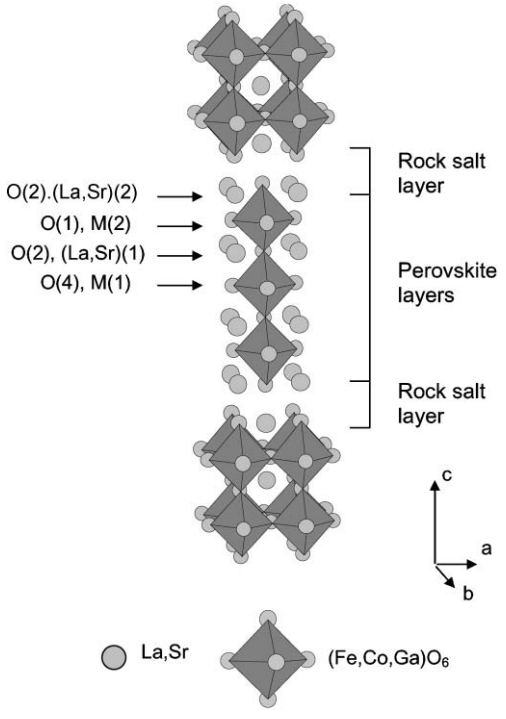

Fig. 1 Crystal structure of tetragonal $LaSr_3Fe_3O_{10-\delta}$.

†Present address: Centro Atómico Bariloche, 8400, S. C. de Bariloche, Argentina.

 DOI: 10.1039/b203778e

of Ga was reported to be $0 < x < 2$ in $LaSr_3Fe_{3-x}Ga_xO_{10-\delta}$.[12] Although the replacement of Fe by Ga increases the oxygen nonstoichiometry, which may be beneficial for oxide-ion conductivity, it is anticipated to decrease the electrical conductivity. However, the decrease in electrical conductivity could be suppressed by a simultaneous substitution of both Co and Ga for Fe, as Co substitution for Fe in $LaSr_3Fe_{3-x}Co_xO_{10-\delta}$ is known to increase the electrical conductivity.[11] In essence, such a simultaneous substitution can increase the oxygen nonstoichiometry without significantly inhibiting electrical conductivity. Accordingly, we investigate here the synthesis, crystal chemistry, and electrical, oxygen permeation, and magnetic properties of the intergrowth phases $LaSr_3GaFe_{2-x}Co_xO_{10-\delta}$ with $0 \leqslant x \leqslant 2$. Additionally, the crystal chemistry of the $LaSr_3GaFe_{2-x}Co_xO_{9-x/2}$ phases obtained by reduction of the parent phases with H_2 is also presented for $x = 0$, 1 and 2.

Experimental

The $LaSr_3GaFe_{2-x}Co_xO_{10-\delta}$ samples with $0 \leqslant x \leqslant 2$ were prepared by solid state reactions of $SrCO_3$, Fe_2O_3, Co_3O_4, and Ga_2O_3. The required quantities of the raw materials were ground and fired first at 1000 °C for 24 h in air. The resulting powders were then reground, pressed into pellets, and fired in air at 1200–1400 °C for 24 h. The melting temperature was found to decrease with the Co content, and so the final firing temperature was lowered from 1420 °C for $x = 0$ to 1200 °C for $x = 2$. The intermediate compositions had a final firing temperature of 1350, 1325, and 1250 °C for $x = 0.5$, 1, and 1.5 respectively. After heating at the final firing temperatures, the samples were kept at 900 °C for 1 h, cooled at a rate of 1 °C min^{-1} to 500 °C, maintained at this temperature for 6 h, and then cooled to room temperature at a rate of 1 °C min^{-1}.

The samples were characterized by X-ray powder diffraction recorded with a Phillips APD 3520 diffractometer using Cu-Kα radiation and a graphite monochromator. The X-ray data were collected from $2\theta = 10$ to 100° with a counting time of 5 s per 0.02°, and refined by the Rietveld method with the DBWS-9411 program.[13] The high temperature X-ray patterns were recorded by spreading the samples on a resistively heated platinum ribbon mounted in an Edmund Bühler HDK 1.4 chamber coupled to a Scintag X1 diffractometer. The oxidation state of (Fe,Co) and the oxygen content were determined by iodometric titration.[14] Thermogravimetric analysis (TGA) plots were recorded with a Perkin-Elmer Series 7 thermal analyzer with a heating rate of 1 °C min^{-1} in flowing air, N_2, or a mixture of 90% Ar and 10% H_2; the gases used had a purity of >99.99%. High temperature ($373 \leqslant T \leqslant 1213$ K) conductivity measurements were carried out in air with disc samples using a four-probe dc technique with the Van der Pauw configuration. Oxygen permeation measurements were carried out with sintered, polished discs having a thickness of about 1.5 mm and densities >90% of theoretical density. Measurements involved exposure of one side of the disc to air (pO_2') and the other side to a lower oxygen partial pressure (pO_2''), controlled by flowing He, and measurement of the oxygen flux with an SRI 8610C gas chromatograph.[15] Magnetic measurements were carried out with a Quantum Design SQUID magnetometer in the temperature range $5 \leqslant T \leqslant 320$ K.

Results and discussion

1 Crystal chemistry

Fig. 2 shows the X-ray powder diffraction patterns of the $LaSr_3GaFe_{2-x}Co_xO_{10-\delta}$ samples for $0 \leqslant x \leqslant 2$. All the patterns could be indexed on the basis of an orthorhombic unit cell similar to that reported for the $LaSr_3GaFe_2O_{10-\delta}$ phase,[12] which is an $n = 3$ member of the R–P series. The orthorhombic

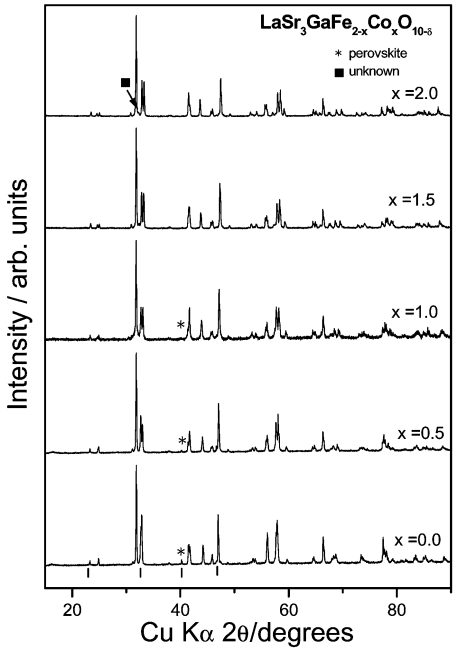

Fig. 2 X-Ray powder diffraction patterns of the $LaSr_3GaFe_{2-x}Co_xO_{10-\delta}$ samples with $0 \leqslant x \leqslant 2$. Since some of the reflections of the secondary perovskite phase overlap with that of the R–P phase, the first four reflections of the perovskite phase are indicated by marks at the bottom of the figure below the pattern of the $x = 0$ sample.

distortion is a consequence of the Ga substitution for Fe. A negligible amount of a secondary perovskite phase was observed for samples with $0 \leqslant x \leqslant 1$ as indicated by a weak reflection around $2\theta = 40$ °. For $x = 1.5$ and 2, a weak reflection corresponding to an unidentified phase was detected around $2\theta = 32$°. The compositions synthesized in this study are indicated by circles and asterisks in the ternary diagram shown in Fig. 3, in which the axes represent the fractions of Fe, Co, and Ga in the B site, with a constant A site composition of $LaSr_3$. In addition, the compositions previously reported in the literature in the series $LaSr_3Fe_{3-x}Co_xO_{10-\delta}$ with $0 \leqslant x \leqslant 1.5$[11] and $LaSr_3Fe_{3-x}Ga_xO_{10-\delta}$ with $0 \leqslant x \leqslant 2.0$[12] are indicated on the Fe–Co and Fe–Ga lines, respectively, with filled squares and triangles. A tentative boundary between the orthorhombic and tetragonal phases is indicated. Attempts to prepare $LaSr_3Ga_{3-x}Co_xO_{10-\delta}$ samples with $x > 2$ or $x < 2$ (indicated by asterisks on the Ga–Co line) resulted in the formation of increasing amounts of secondary phases.

The crystal structures of the $LaSr_3GaFe_{2-x}Co_xO_{10-\delta}$ samples with $0 \leqslant x \leqslant 2$ were refined by the Rietveld method on the basis of the orthorhombic space group *Fmmm*, adopted

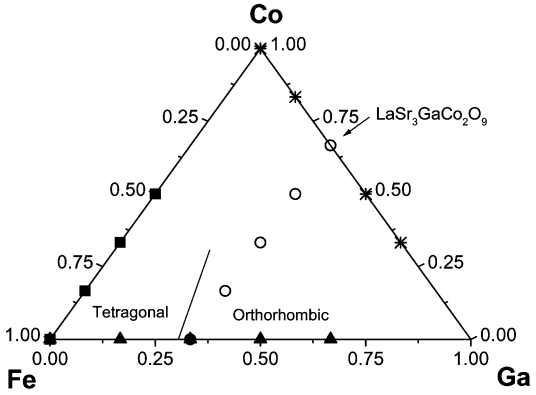

Fig. 3 Schematic ternary Ga–Fe–Co diagram, indicating the location of the samples with various fractions of Ga, Fe or Co in the B site of the $n = 3$ member of the R–P phase $LaSr_3(Ga,Fe,Co)_3O_{10-\delta}$: (■) ref. 12; (▲) ref. 13; (○, *) this work.

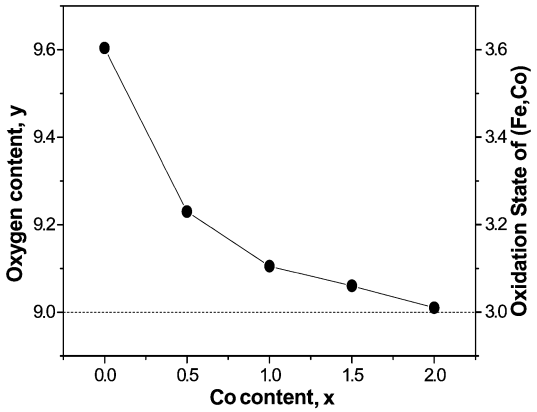

Fig. 4 Variation of the oxygen content and average oxidation state of Fe and Co with Co content in $LaSr_3GaFe_{2-x}Co_xO_{10-\delta}$.

previously for $LaSr_3GaFe_2O_{10-\delta}$.[12] During the refinement, the oxygen contents of the samples were fixed at the values obtained from iodometric titration. Fig. 4 shows the variation of the oxygen content and the average oxidation state of (Fe,Co) with Co content in $LaSr_3GaFe_{2-x}Co_xO_{10-\delta}$. The data show that the oxygen content decreases with increasing Co content from 9.6 at $x = 0$ to 9.0 at $x = 2$, leading to an average oxidation state of 3+ for Co in $LaSr_3GaCo_2O_9$. The errors in the oxygen content values are ± 0.02. The low X-ray scattering factor of oxygen atoms compared to the heavier La and Sr atoms hinder us from determining precisely the position of the oxygen vacancies in the crystal lattice using X-ray diffraction. Nevertheless, in analogy with other $n = 3$ R–P phases, such as $LaSr_3Fe_3O_{10-\delta}$,[10] $LaSr_3FeGa_2O_{10-\delta}$,[12] $Ca_4Mn_2FeO_{9.75}$[16] and $Sr_4Mn_2FeO_{9.8}$,[16] the oxygen vacancies are most probably located at the O(2) and O(4) sites. Accordingly, the oxygen vacancy concentration obtained from the wet iodometric titration data was distributed evenly between the O2 and O4 sites and the O1 and O3 sites were kept at full occupancy in our refinement of the crystal structure. The observed and calculated profiles and the difference between the two for $LaSr_3GaCo_2O_9$ with Co^{3+} are shown in Fig. 5. The refined structural parameters for $LaSr_3GaCo_2O_9$ are listed in Table 1.

The lattice parameters of the $LaSr_3GaFe_{2-x}Co_xO_{10-\delta}$ samples with $0 \leqslant x \leqslant 2.0$ that were annealed in air are given in Table 2. While the *a* and *b* parameters decrease with increasing Co content, the *c* parameter increases, with a net decrease in cell volume as the Co content increases. Also, the orthorhombic distortion in the *a*–*b* plane increases with Co content and it tends to saturate at about 1.15% for $x \geqslant 1.5$. While the decrease in the *a* and *b* parameters can be understood by

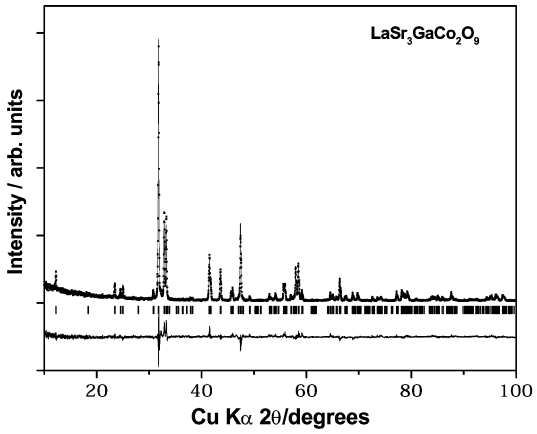

Fig. 5 Observed and calculated X-ray diffraction data and the difference between them for $LaSr_3GaCo_2O_9$ at room temperature. The positions of the reflections are also marked.

Table 1 Structural parameters of $LaSr_3GaCo_2O_9$ at room temperature[a]

Atom	Site	Occupancy	*x*	*y*	*z*
(¼ La, ¾ Sr)1	8i	1	0	0	0.579(1)
(¼ La, ¾ Sr)2	8i	1	0	0	0.701(1)
(1/3 Ga, 2/3 Co)1	4a	1	0	0	0
(1/3 Ga, 2/3 Co)2	8i	1	0	0	0.145(2)
O1	16j	1	¼	¼	0.139(5)
O2	8i	0.75[b]	0	0	0.070(5)
O3	8i	1	0	0	0.215(6)
O4	8e	0.75[b]	¼	0	0

[a]Space group: *Fmmm*; $a = 5.393(1)$, $b = 5.456(1)$, $c = 29.080(5)$ Å, $V = 855.68(3)$ Å^3. $R_{wp} = 13.07\%$, $R_p = 10.41\%$, $S = 2.86$. [b]The oxygen vacancies were located at the O2 and O4 sites, in analogy with the previous data in the literature.[10,12,16] The oxygen vacancy concentration was distributed evenly between the two sites (O2 and O4 sites) and the occupancies for the O2 and O4 sites were fixed based on the oxygen content values obtained from the iodometric titration.

considering the substitution of a smaller $Co^{3+/4+}$ for $Fe^{3+/4+}$, the increase in the *c* parameter necessitates consideration of the change in cationic size as well as the increase in the oxygen vacancy concentration.

With respect to oxide-ion conductivity, the $LaSr_3Fe_{3-x}Co_xO_{10-\delta}$ and $La_{0.3}Sr_{2.7}Fe_{2-x}Co_xO_{7-\delta}$ systems exhibit oxygen permeation flux values of the same magnitude as some of the perovskite phases, *e.g.* $La_{0.4}Sr_{0.6}Co_{0.8}Fe_{0.2}O_{3-\delta}$ and $SrFe_{0.75}Co_{0.25}O_{3-\delta}$.[17,18] However, in the case of the presently investigated $LaSr_3GaFe_{2-x}Co_xO_{10-\delta}$ system, the observed orthorhombic distortion may represent an important drawback to the oxide-ion conductivity. As a simple rule, for ionic conduction, the crystal structure must provide partially occupied equivalent crystallographic sites for the mobile ions to move.[19] For example, the perovskite phase $SrCo_{0.8}Fe_{0.2}O_{3-\delta}$ exhibits an increment in the oxygen permeation flux value with increasing temperature associated with a structural transformation from an oxygen vacancy-ordered brownmillerite structure (orthorhombic symmetry) to a vacancy-disordered cubic structure.[20]

With the objective of evaluating the structural behavior of the Co-rich samples of the presently investigated system, we performed high temperature X-ray diffraction measurements in air on the $LaSr_3GaCo_2O_{9.0}$ phase. The sample maintains the orthorhombic symmetry from room temperature to 900 °C. Both the *a* and *b* parameters increase with temperature and the degree of orthorhombic distortion does not show any change. Similarly, the *c* parameter and the unit cell volume also increase with temperature. The thermal expansion coefficients for the three crystallographic directions were computed from X-ray diffraction data. The obtained values are 11.9×10^{-6} K^{-1} in the *a*–*b* plane and 13.6×10^{-6} K^{-1} along the *c*-axis. These values are slightly higher than the thermal expansion coefficient of yttria-stabilized zirconia (10.3×10^{-6} K^{-1}), which is used as an electrolyte in solid oxide fuel cells (SOFC), but similar to those of the perovskite phases $La_{1-x}Sr_xMnO_3$[2] that are used as cathodes in SOFC.

Table 2 Lattice parameters, unit cell volume, and orthorhombic distortion in the a–b plane of $LaSr_3GaFe_{2-x}Co_xO_{10-\delta}$ at room temperature

x	*a*/Å	*b*/Å	*c*/Å	*V*/Å^3	$(a-b)/b$ (%)
0.0	5.465(1)	5.492(1)	28.74(1)	862.6(3)	0.50
0.5	5.446(1)	5.495(1)	28.82(1)	862.4(3)	0.91
1.0	5.425(1)	5.482(1)	28.87(1)	858.5(3)	1.11
1.5	5.409(1)	5.471(1)	29.00(1)	858.2(3)	1.15
2.0	5.394(1)	5.455(1)	29.08(1)	855.7(3)	1.13

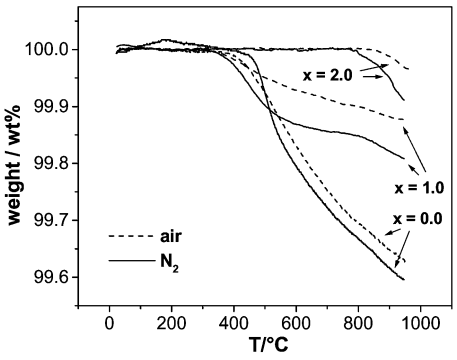

Fig. 6 TGA plots of $LaSr_3GaFe_{2-x}Co_xO_{10-\delta}$ recorded in nitrogen and air with a heating rate of 1 °C min^{-1}.

2 Variation of oxygen content with temperature

The variation of the oxygen contents of the $LaSr_3GaFe_{2-x}Co_xO_{10-\delta}$ ($0 \leqslant x \leqslant 2$) samples with temperature were determined by TGA measurements in air and N_2 (Fig. 6). The samples do not show any weight loss for $T < 400$ °C, indicating that the samples do not lose oxygen up to 400 °C. While the samples with $0 \leqslant x \leqslant 1$ lose oxygen for $T > 400$ °C both in air and N_2 atmospheres, the $x = 2$ sample does not show any oxygen loss up to 800 °C. The stability of the $x = 2$ sample compared to the other samples with lower Co contents is due to a lower oxidation state of around 3+ for Co in the former (Fig. 4). The loss of oxygen at $T > 800$ °C in the $x = 2$ sample is due to a reduction of some of the Co^{3+} ions to Co^{2+}, as we will see later during the reduction in a mixture of 90% Ar and 10% H_2. At a given temperature, the amount of oxygen loss decreases with increasing Co content; for example, the weight loss decreases from 0.38 wt% for $x = 0$ to 0.05 wt% for $x = 2.0$ at 900 °C in N_2.

3 Electrical conductivity

Arrhenius plots of the variation of electrical conductivity (σ) with temperature for $LaSr_3GaFe_{2-x}Co_xO_{10-\delta}$ ($0 \leqslant x \leqslant 2$) in air in the temperature range $450 \leqslant T \leqslant 1200$ K are shown in Fig. 7. All the samples show thermally activated behavior at low temperature, and an activation energy was computed from the linear range of the plots ($330 \leqslant T \leqslant 570$ K). One of the insets in Fig. 7 shows that the activation energy increases with Co content from 0.17 at $x = 0$ to 0.3 eV at $x = 2$. The electrical conductivity *versus* temperature plot of the $x = 0$ sample exhibits a maximum at about $T = 400$ °C, which corresponds to the start of oxygen loss from the structure, as seen in the

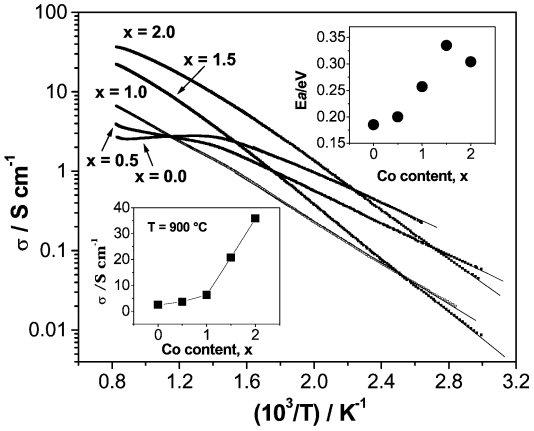

Fig. 7 Variation of the electrical conductivity of $LaSr_3GaFe_{2-x}Co_xO_{10-\delta}$ ($0 \leqslant x \leqslant 2.0$) with temperature in air. The upper and lower insets show, respectively, the variation with Co content of the activation energy computed from data in the temperature range $330 \leqslant T \leqslant 570$ K and the electrical conductivity at $T = 900$ °C.

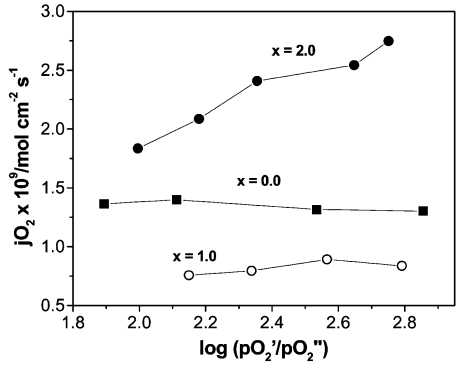

Fig. 8 Variations of oxygen permeation flux of $LaSr_3GaFe_{2-x}Co_xO_{10-\delta}$ with log (pO_2'/pO_2''). The measurements were conducted at 900 °C with 1.5 mm thick samples.

TGA plot (Fig. 6). The decrease in conductivity at higher temperature $T > 400$ °C is due to a decrease in the carrier concentration caused by the loss of oxygen. Although the other samples with $x = 0.5$ and 1 do not show any distinct maximum, the slope of the curve changes around 400 °C due to the oxygen loss from the lattice. The change in the slope becomes less pronounced as the Co content increases due to the decreasing amount of oxygen loss. The variation of σ with Co content at a fixed temperature of 900 °C is displayed in the lower inset of Fig. 7. The electrical conductivity increases by approximately one order of magnitude from 2 to 36 S cm^{-1} at 900 °C on increasing the Co content from $x = 0$ to $x = 2$. However, at lower temperatures, the Fe-rich samples have higher conductivity due to the higher oxygen content and oxidation state of (Fe,Co), which is also reflected in a lower activation energy (inset in Fig. 7) of the thermally activated process. The electrical conductivity values at high temperature ($T > 800$ °C) of the $LaSr_3GaFe_{2-x}Co_xO_{10-\delta}$ samples with high Co content ($1.5 \leqslant x \leqslant 2$) are lower than those obtained for the $LaSr_3Fe_{3-x}Co_xO_{10-\delta}$ phases without Ga,[11] but similar to the values reported for the $n = 2$ member of the R–P phases $La_{0.3}Sr_{2.7}Fe_{2-x}Co_xO_{7-\delta}$ with $0.0 \leqslant x \leqslant 1$.[17]

4 Oxygen permeation properties

Fig. 8 shows the variation of oxygen permeation flux (jO_2) as a function of the oxygen partial pressure gradient log (pO_2'/pO_2'') at a constant temperature of $T = 900$ °C for 1.5 mm thick $LaSr_3GaFe_{2-x}Co_xO_{10-\delta}$ ($0 \leqslant x \leqslant 2$) disks. The samples exhibit jO_2 values of the order of 10^{-9} mol s^{-1} cm^{-2}, without any particular trend with Co content. The flux values are 2 orders of magnitude lower than those obtained for other R–P phases such as $La_{0.3}Sr_{2.7}Fe_{2-x}Co_xO_{7-\delta}$ ($n = 2$ member) and $LaSr_3Fe_{3-x}Co_xO_{10-\delta}$ ($n = 3$ member).[11,17] Due to the low oxygen permeation rates of the $LaSr_3GaFe_{2-x}Co_xO_{10-\delta}$ membranes, the oxygen partial pressure measurements of pO_2'' were at the detection limit of our gas chromatograph. We believe that the low oxygen permeation flux values in spite of a significant amount of oxygen vacancies in the structure is due to the orthorhombic distortion and the very low oxygen concentration gradient across the membrane. As evident from the TGA data in Fig. 6, the difference in the oxygen content values between air and N_2 atmosphere at a given temperature (for example, 900 °C) is very small, which results in a negligible oxygen vacancy concentration gradient from the high pO_2 side (air) to the low pO_2 side across the membrane. The low oxygen concentration gradient leads to poor driving force for oxygen permeation and, thereby, low oxygen permeation flux values.

5 Chemical stability in reducing atmospheres

With the objective of evaluating the chemical stability of the $LaSr_3GaFe_{2-x}Co_xO_{10-\delta}$ phases, we carried out TGA

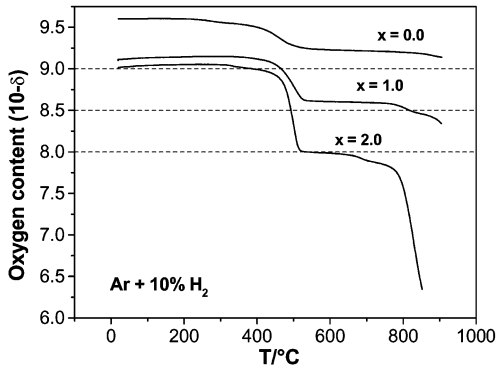

Fig. 9 Variations of the oxygen content of $LaSr_3GaFe_{2-x}Co_xO_{10-\delta}$ with temperature in a mixture of 90% Ar and 10% H_2. The plots were derived using the room temperature oxygen content values obtained from the iodometric titration and the TGA data collected in a mixture of 90% Ar and 10% H_2.

measurements in a mixture of 90% Ar and 10% H_2. The variation of the oxygen content with temperature are shown in Fig. 9. The room temperature oxygen content values given in Fig. 9 were determined by iodometric titration (Fig. 4). All the samples begin to lose oxygen above about 400 °C. The $x = 0$ sample shows a plateau at $T > 500$ °C, corresponding to the formation of $LaSr_3GaFe_2O_{9.2}$. The plateau extends to high temperatures (900 °C) and no evidence of decomposition was detected. The samples with $x = 1$ and 2 also show a plateau at $T > 500$ °C, corresponding to the formation of the phases $LaSr_3GaFeCoO_{8.6}$ and $LaSr_3GaCo_2O_{8.0}$, respectively, with an oxidation state of +2 for Co, assuming +3.2 for Fe. However, the $x = 2.0$ sample exhibits a dramatic decrease in oxygen content around $T = 800$ °C due to the decomposition of the sample at high temperatures. The data indicate that the chemical stability in reducing atmospheres decreases with increasing Co content.

Fig. 10 shows the X-ray diffraction patterns of the $LaSr_3GaFe_{2-x}Co_xO_{9-x/2}$ samples that were obtained after heating the samples in a mixture of 90% Ar and 10% H_2 to the plateau regions of the TGA plots in Fig. 9. A comparison of the X-ray patterns with those recorded before the reduction (Fig. 2) indicates that the new phases also preserve the orthorhombic symmetry. The crystal structures of these phases

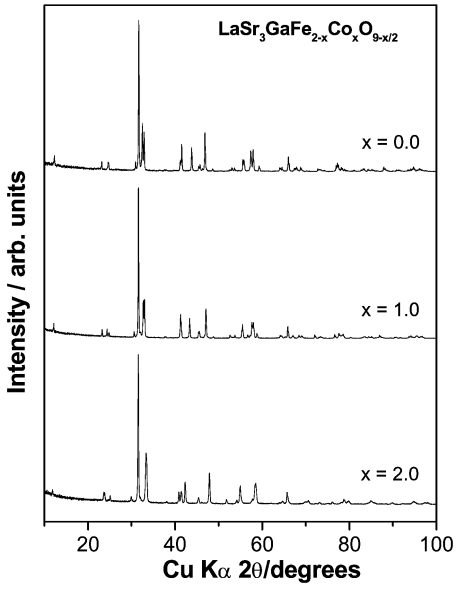

Fig. 10 X-Ray powder diffraction patterns of the $LaSr_3GaFe_{2-x}Co_xO_{9-x/2}$ samples that were obtained after heating to the plateau regions in the TGA plots of Fig. 9 in a mixture of 90% Ar and 10% H_2.

Table 3 Lattice parameters and unit cell volume of $LaSr_3GaFe_{2-x}Co_xO_{9-x/2}$

x	a/Å	b/Å	c/Å	V/Å^3
0	5.455(1)	5.521(1)	28.959(5)	872.0(3)
1.0	5.438(1)	5.483(1)	29.241(5)	871.9(3)
2.0	5.364(1)	5.395(1)	29.919(5)	865.9(3)

were, therefore, refined by the Rietveld method based on the structural model used earlier for $LaSr_3GaCo_2O_9$ (see Table 1). The lattice parameters and unit cell volume are listed in Table 3. The oxygen vacancies are known to be localized mainly in the O(2) sites in the analogous $Ln_4Ni_3O_8$ (Ln = La, Nd) phases that were obtained by a reduction of $Ln_4Ni_3O_{10}$, resulting in a 4-fold coordination for $Ni^{+/2+}$ in $Ln_4Ni_3O_8$.[21,22] Also, the LnO–LnO rock-salt layers rearrange to give an Ln_2O_2 fluorite arrangement in $Ln_4Ni_3O_8$. Unlike the $Ln_4Ni_3O_8$ phases, the $LaSr_3GaFe_{2-x}Co_xO_{9-x/2}$ phases maintain the original orthorhombic crystal structure without any structural change as both iron and cobalt do not prefer square coplanar coordination. This observation suggests that the oxygen deficiency may not be constrained to the O(2) sites in $LaSr_3GaFe_{2-x}Co_xO_{9-x/2}$. Nevertheless, further detailed study with neutron diffraction is needed to locate precisely the distribution of oxygen vacancies in the $LaSr_3GaFe_{2-x}Co_xO_{9-x/2}$ phases.

6 Magnetic properties

The variation of the inverse molar magnetic susceptibility with temperature for the $LaSr_3GaFe_{2-x}Co_xO_{10-\delta}$ samples is shown in Fig. 11. The magnetic measurements were carried out both under zero-field-cooled (zfc) and field-cooled (fc) conditions with a magnetic field of 0.1 T. The Weiss constant obtained from the linear extrapolation of the high-temperature region (220–320 K) is negative for all the samples, indicating antiferromagnetic interactions. However, no Neel temperature could be determined from our measurements. The magnetic moment μ_{eff} obtained from the slope of the linear extrapolation varies from 5.15 μ_B for $LaSr_3GaFe_2O_{9.6}$ to 4.77 μ_B for $LaSr_3GaCo_2O_{9.0}$. The μ_{eff} value (4.77 μ_B) obtained for the $x = 2$ sample agrees closely with that expected (4.89 μ_B) for high spin Co^{3+} ($t^4_{2g}\ e^2_g$) ($S = 2$). Also, the μ_{eff} value (5.15 μ_B) obtained for the $x = 0$ sample is close to that (5.34 μ_B) expected based on the coexistence of 40% high spin Fe^{3+} and 60% Fe^{4+} according to the experimentally determined oxygen content. The inset in Fig. 11 shows the variation of the molar magnetic susceptibility with temperature. The presence of a maximum only in the zfc curves at around $T = 50$ K suggests spin-glass behavior without long-range magnetic ordering.

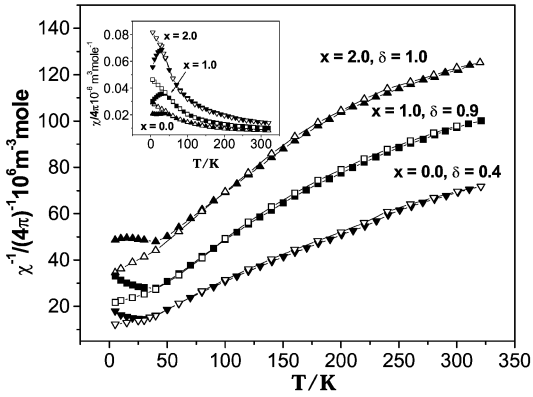

Fig. 11 Variation of the inverse molar magnetic susceptibility of $LaSr_3GaFe_{2-x}Co_xO_{10-\delta}$ with temperature. The inset shows the variation of molar magnetic susceptibility with temperature.

Conclusions

The $n = 3$ member of the R–P phase, $LaSr_3GaFe_{2-x}Co_xO_{10-\delta}$, has been synthesized for $0 \leqslant x \leqslant 2$. The samples have an orthorhombic structure (space group *Fmmm*) that is isotypic with the $LaSr_3GaFe_2O_{10-\delta}$ phase. The oxygen content decreases with increasing Co content. The samples exhibit a thermally activated conduction process with the activation energy increasing with Co content. The samples exhibit low oxygen permeation flux values that are 2 to 3 orders of magnitude lower than those of the other R–P phases, such as $LaSr_3Fe_{3-x}Co_xO_{10-\delta}$ and $La_{0.3}Sr_{2.7}Fe_{2-x}Co_xO_{7-\delta}$, due to the negligible oxygen vacancy concentration gradient across the membranes and the orthorhombic crystal symmetry. The samples yield orthorhombic $LaSr_3GaFe_{2-x}Co_xO_{9-x/2}$ phases with Co^{2+} upon reduction with H_2. The $LaSr_3GaFe_{2-x}Co_xO_{10-\delta}$ samples exhibit weak antiferromagnetic interactions with high spin Co^{3+}.

Acknowledgement

Financial support by the Welch Foundation, grant no. F-1254, is gratefully acknowledged. Two of the authors, F. P. and K. G., thank CONICET, Argentina, and BOYSCAST, India, respectively, for postdoctoral fellowships.

References

1 H. J. Bouwmeester and A. J. Burggraaf, in *The CRC Handbook of Solid State Electrochemistry*, ed. P. J. Gellings and H. J. Bouwmeester, CRC Press, Boca Raton, 1997, ch. 14.
2 N. Q. Minh, *J. Am. Ceram. Soc.*, 1993, **76**, 563.
3 Y. Teraoka, H. M. Zhang, S. Furukawa and N. Yamazoe, *Chem. Lett.*, 1985, 1743.
4 Y. Teraoka, T. Nobunaga and N. Yamazoe, *Chem. Lett.*, 1988, 503.
5 Y. Teraoka, H. M. Zhang, K. Okamoto and N. Yamazoe, *Mater. Res. Bull.*, 1988, **23**, 51.
6 S. N. Ruddlesden and P. Popper, *Acta Crystallogr.*, 1958, **11**, 54.
7 S. E. Dann, M. T. Weller and D. B. Currie, *J. Solid State Chem.*, 1992, **97**, 179.
8 S. E. Dann, M. T. Weller, D. B. Currie, M. F. Thomas and A. D. Al-Rawwas, *J. Mater. Chem.*, 1993, **3**, 1231.
9 C. Brisi and P. Rolando, *Ann. Chim. (Rome)*, 1969, **59**, 385.
10 J. Y. Lee, J. S. Swinnea, H. Steinfink, W. M. Reiff, S. Pei and J. D. Jorgensen, *J. Solid State Chem.*, 1993, **103**, 1.
11 T. Armstrong, F. Prado and A. Manthiram, *Solid State Ionics*, 2001, **140**, 89.
12 B. Shankar and H. Steinfink, *J. Solid State Chem.*, 1996, **122**, 390.
13 R. A. Young, A. Sakthivel, T. S. Moss and C. O. Paiva Santos, *J. Appl. Crystallogr.*, 1995, **28**, 366.
14 A. Manthiram, J. S. Swinnea, S. T. Sui, H. Steinfink and J. B. Goodenough, *J. Am. Chem. Soc.*, 1987, **109**, 6667.
15 T. Armstrong, F. Prado, Y. Xia and A. Manthiram, *J. Electrochem. Soc.*, 2000, **147**, 435.
16 P. D. Battle, W. R. Branford, A. Mihut, M. J. Rosseinsky, J. Singleton, J. Sloan, L. E. Spring and J. F. Vente, *Chem. Mater.*, 1999, **11**, 674.
17 F. Prado, T. Armstrong, A. Caneiro and A. Manthiram, *J. Electrochem. Soc.*, 2001, **148**, J7.
18 A. Manthiram, F. Prado and T. Armstrong, *Solid State Ionics*, in press.
19 J. B. Goodenough, *Proc. R. Soc. London, A*, 1984, **393**, 215.
20 H. Kruidhof, H. J. M. Bouwmeeester, R. H. E. v. Doorn and A. J. Burggraaf, *Solid State Ionics*, 1993, **63–65**, 816.
21 Ph. Lacorre, *J. Solid State Chem.*, 1993, **97**, 495.
22 A. Manthiram, J. P. Tang and V. Manivannan, *J. Solid State Chem.*, 1999, **148**, 499.